Macromolecules
ARTICLE

Macromolecules **2010**, *43*, 8079–8085 **8079**
DOI: 10.1021/ma101531k

Ultraporous Films with Uniform Nanochannels by Block Copolymer Micelles Assembly

Suzana P. Nunes,[†] Rachid Sougrat,[‡] Bobby Hooghan,[§] Dalaver H. Anjum,[§] Ali Reza Behzad,[‡] Lan Zhao,[‡] Neekalanda Pradeep,[†] Ingo Pinnau,[†] Ulla Vainio,[⊥] and Klaus-Viktor Peinemann*[,†]

[†]*Advanced Membranes and Porous Materials Center at KAUST,* [‡]*Advanced Nanofabrication, Imaging and Characterization Lab at KAUST, and* [§]*FEI at KAUST, King Abdullah University of Science and Technology (KAUST), Thuwal 23955-6900, Kingdom of Saudi Arabia, and* [⊥]*HASYLAB at Deutsches Elektronen-Synchrotron (DESY), D-22607 Hamburg, Germany*

Received July 9, 2010; Revised Manuscript Received August 22, 2010

ABSTRACT: Films with high pore density and regularity that are easy to manufacture by conventional large-scale technology are key components aimed for fabrication of new generations of magnetic arrays for storage media, medical scaffolds, and artificial membranes. However, potential manufacture strategies like the self-assembly of block copolymers, which lead to amazing regular patterns, could be hardly reproduced up to now using commercially feasible methods. Here we report a unique production method of nanoporous films based on the self-assembly of copper(II) ion−polystyrene-*b*-poly(4-vinylpyridine) complexes and nonsolvent induced phase separation. Extremely high pore densities and uniformity were achieved. Water fluxes of 890 L m^{-2} h^{-1} bar^{-1} were obtained, which are at least 1 order of magnitude higher than those of commercially available membranes with comparable pore size. The pores are also stimuli (pH)-responsive.

Introduction

Films with ultrahigh density of monodispersed pores easily produced in technical scale would bring a breakthrough in technologies varying from artificial membranes for water treatment,[1,2] medical processes,[3] data storage, and electronics.[4−6] The miniaturization of devices for magnetic storage and optoelectronics depends on the availability of ultrahigh-density arrays, which become difficult to produce when the patterns approach the nanoscale. Innovative manufacture of nanowires has been proposed by electrodeposition in block copolymer templates.[5] However, the template technical manufacture is still a challenge. One of the most relevant applications for nanoporous films is water purification. Water supplies are suffering worldwide from growing contamination caused by human activity, including a variety of hormones, antibiotics, and endocrine disrupters.[1,2] Effective decontamination would require much higher fluxes and narrow pore size distribution in the range of nano- and ultrafiltration aligned to low fouling sensitivity. Medical processes like hemodialysis[3] could be substantially shortened with high flux membranes. However, a sharp control of pore size is required to ensure the health of the patients, which currently spend hours for each day of treatment. The commercial membranes for water purification still mostly resemble the asymmetric porous films developed in the 1960s.

In this report we describe a unique approach to technical production of nanoporous films inspired by the self-assembly of block copolymers,[7] metal-directed supramolecular[8] chemistry, and nonsolvent induced phase separation. Diblock copolymers spontaneously form regular patterns on nanometer scale through minimization of free energy.[4] The potential of block copolymers for preparation of nanoporous films has been recognized.[9−15] A bottleneck is certainly reproducible in large scale. The primordial issue is the fact that in many cases the most convenient morphology is not that expected in equilibrium, and this is frequently not considered in previous developments.[13] First of all, block copolymers assembly in a myriad of morphologies in solution,[16] offering innumerous possibilities for tailoring nanostructures. The micelles and vesicles formed in solution are however very dynamic, and as soon as the solvent is evaporated the morphology is transformed. Controlling and stabilizing morphologies far from equilibrium is the key challenge in the bottom-up nanostructure fabrication. The film morphology is not only dependent on the thermodynamic interaction between blocks but also on a series of factors, including the viscosity and the presence of impurities, which dramatically influences the kinetics of phase separation and self-assembly. Abrupt phase separation by immersion in a nonsolvent bath, known as "phase inversion", has been used for decades to freeze incipient porous structures in the manufacture of commercial membranes. In this paper metal−polymer complexation is used as method for directing self-assembly, stabilizing micelles in solution and providing intermicellar cross-linking. This process combined with "phase inversion" in water gives rise to an exceptionally ordered porous structure with a reproducibility not reported before. The self-assembly in solution and its influence on the mechanism of pore formation were understood with help of synchrotron X-ray scattering and a series of advanced microscopy methods.

Experimental Section

Materials. Polystyrene-*b*-poly(4-vinylpyridine) block copolymer P5722P (PS-*b*-P4VP, 138 000-*b*-41 0000 g/mol) and poly(4-vinylpyridine) (P4VP) M_w 42 500 g/mol and M_n 36 300 g/mol were purchased from Polymer Source, Inc., Canada. Copper acetate was supplied by Aldrich, as well as dimethylformamide (DMF) and tetrahydrofuran (THF).

Porous Film Preparation. Films were mostly cast from polymer solutions containing 20 wt % PS-*b*-P4VP block copolymer (except in the films of Figure 8) in a mixture of 56 wt % *N*,*N*-dimethylformamide (DMF) and 24 wt % tetrahydrofuran

*Corresponding author: Tel +966 2 8082769; e-mail klausviktor.peinemann@kaust.edu.sa.

Published on Web 09/03/2010

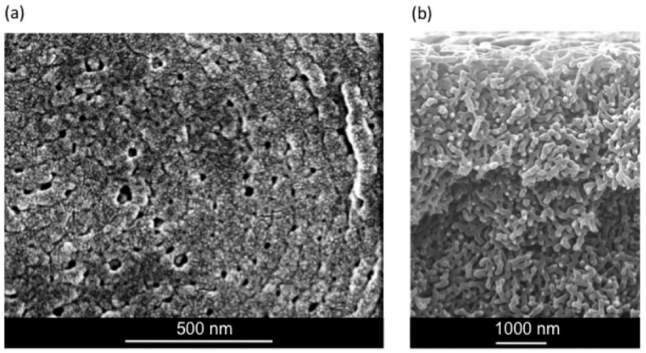

Figure 1. Microscopy of a membrane cast from 20% PS-*b*-P4VP solution with 56% DMF and 24% THF.

(THF). For films shown in Figure 7 the THF/DMF concentration was varied as specified. The solvent was let to evaporate during up to 20 s (except in Figure 8), and the film was immersed in water at room temperature. Membranes were prepared by adding 0.15 wt % copper(II) acetate to the casting solution (except in Figure 1). Most membranes were cast on glass plates, using casting blades with 200 μm gate height. The scale-up was performed by analogously casting the solutions on Hirose TH100 polyester support. The room temperature was about 20 °C with 60% relative humidity.

P4VP Film Preparation. The poly(4-vinylpyridine) (P4VP) film for SAXS and WAXS was prepared by solution casting in ethanol with copper(II) acetate, followed by complete solvent evaporation.

Water Flux and pH Response Characterization. The water flux was measured under different pH values using an Amicon cell with testing area ca. 5 cm^2 at 1 bar. Acid solutions were prepared with different concentrations of nitric acid. Basic solutions were prepared with different concentrations of sodium hydroxide. The pH values were confirmed with a pH-meter, just before the experiments.

Small-Angle and Wide-Angle X-ray Scattering (SAXS and WAXS). SAXS and WAXS of a PS(138K)-*b*-P4VP(41K) block copolymer membrane and a film of P4VP homopolymer, both complexed with copper acetate, were measured at beamline B1 at DORIS synchrotron in HASYLAB at DESY, in Hamburg. SAXS measurements were made at four different photon energies near the Cu K edge E = 8887, 8966, 8978, and 8984 eV. The SAXS signal was measured using a 2D single photon counting Pilatus 300k detector at two different sample-to-detector distances of 0.885 and 3.585 m. The length of the scattering vector is defined in the following report as $q = 4\pi \sin\theta/\lambda$, where θ is half of the scattering angle.

The WAXS measurements were made at photon energy E = 16 keV using a 1D Mythen strip detector, which was positioned 133.6 mm behind the sample. During all measurements, both SAXS and WAXS, the samples were in vacuum ($P < 10^{-4}$ mbar).

All samples were cut and several layers of film were stacked for the measurement giving a total thicknesses of 0.43 mm for the block copolymer and 0.185 mm for the homopolymer sample. SAXS and WAXS measurements were corrected for absorption and background scattering and normalized to absolute intensity units using a glassy carbon reference sample. The effect of form factor from the spheres was simulated by using the program Scatter.

Electron Microscopy. *Morphological Investigation of the Casting Solution*. Two methods were used to confirm the presence of block copolymer micelles stabilized by complexation with copper ions in a mixture of THF and DMF: cryo-transmission and cryo-field emission scanning electron microscopy.

Cryo-Transmission Electron Microscopy (*Cryo-TEM*). A sample of the casting solution was deposited on a Quantifoil grid (Quantifoil Inc., Jena, Germany) and plunge-frozen in

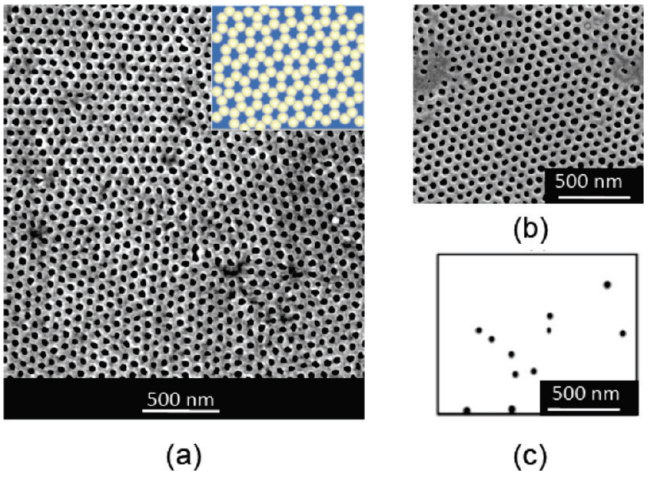

Figure 2. Surface pores in a membrane cast (a) on glass and (b) on polyester nonwoven, from 20% PS-*b*-P4VP solutions with 56% DMF, 24% THF, and 0.15% $Cu(Ac)_2$, immersed in water after 20 s of evaporation. (c) Pore distribution of a track-etched 30 nm polycarbonate membrane according to micrograph reported in ref 30.

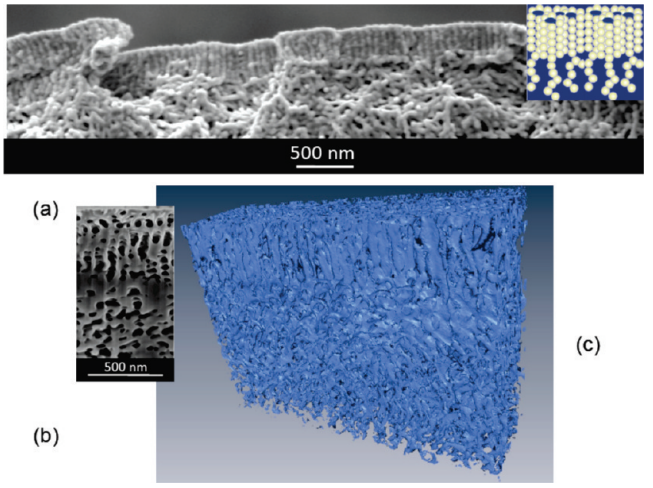

Figure 3. (a) Cross-section (FESEM) and (b) one of 150 FIB slices of a membrane cast from 20% PS-*b*-P4VP solutions with 56% DMF, 24% THF, and 0.15% $Cu(Ac)_2$. (c) In blue a 3D reconstruction of the membrane pores, after assemblying a series of FIB slices.

liquid ethane. Grids were imaged at liquid nitrogen temperatures using a Titan Krios (FEI Co., Hillsboro, OR) equipped with a 2K × 2K CCD placed at the end of Gatan energy filter and operated at 300 kV. Typically, electron doses of ~100 electrons/$Å^2$ were used.

Cryo-Field Emission Scanning Electron Microscopy (*Cryo-FESEM*). Low-temperature experiments were carried out using a Quorum PP2000T cryo-transfer system (Qurorum Technologies, Newhaven, UK) that was fitted to an FEI Nova Nano630 SEM with a field emission electron source and through-lens electron detectors. A small amount of polymer solution was mounted between two rivets secured in a hole on an aluminum stub on the specimen holder. The sample holder, attached to a transfer rod, was then rapidly plunged into liquid nitrogen slush and under vacuum transferred to the preparation chamber precooled at −180 °C and allowed to equilibrate for 10 min. The sample temperature was raised to −160 °C, and a fractured surface was obtained by hitting the top rivet with a knife and removing it from the top surface. The revealed fractured plane was sublimed at −90 °C for 5 min to eliminate any eventually condensed ice. To avoid charging problems, the sample temperature was then reduced to −135 °C and the sample was

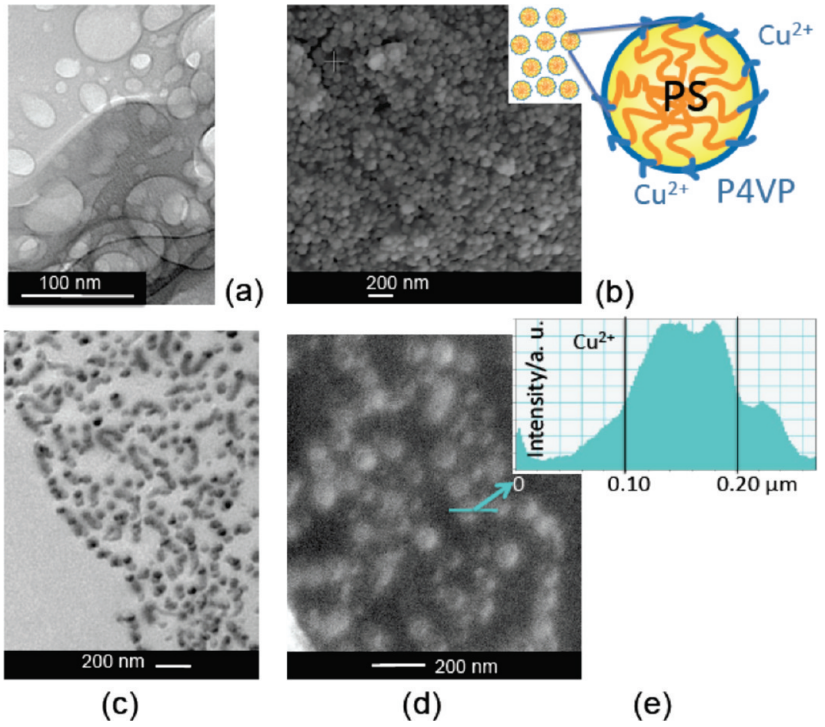

Figure 4. (a) Cryo-TEM and (b) cryo-FESEM of 20% PS-*b*-P4VP solution in 56% DMF, 24% THF, and 0.15% $Cu(Ac)_2$ with schematic representation of micelles in solution. (c) TEM and (d) high-angle annular dark field scanning transmission electron microscopy (HAADF-STEM) of membranes cast from the same solution (taken from an aleatory position in the center of the film). (e) Electron energy loss spectroscopy (EELS) along a line crossing a micelle (74 eV). Contrast is inverted in (d).

sputter-coated with gold−palladium for 90 s at 5 mA current in an argon atmosphere. The sample was then transferred to SEM cryo-stage, which was held at −140 °C. The micrograph is shown in Figure 4b.

Morphological Investigation of the Final Porous Film. The morphology of the obtained film was characterized by different scanning and transmission electron microscopy methods, including focused ion beam.

Field Emission Scanning Electron Microscopy (*FESEM*). The membrane surface and cross section were observed on FEI Quanta 200 and Helios 400S microscopes at 750 V (Figure 1a), 5 kV (Figure 3a) and 30 kV (Figure 2). Before the observation the samples were coated with Au/Pd by sputtering using a K575X Emitech equipment. For cross section the membranes were fractured in liquid nitrogen.

Focused Ion Beam (*FIB*). Membranes were cut using focused ion beam. To minimize the polymer sample damage by the ion beam, the beam currents were lower than usually applied for semiconductors analysis, and a protective Pt layer was deposited, prior to milling the surface at the region of interest. The layer was deposited using ion beam induced CVD, inside the FIB/SEM chamber. In order to effectively dissipate surface charge from the surface, the membrane surface was also sputter-coated with Au prior to imaging/milling.

A series of slices were obtained using a FEI Helios 400S small dual beam system and proprietary Slice & View software. The slice thickness was 15 nm. The series of slices of the membrane prepared with copper salt was assembled to supply a 3D overview of the membrane pore structure. 3D visualization and semiautomated segmentation were carried out using software tools implemented in the program Amira (TGS, San Diego, CA).

Transmission Electron Microscopy (*TEM*). The membrane was embedded in low viscosity Epoxy resin (Agar R1165) and cured at 60 C for 24 h. Ultrathin sections (80 nm) were prepared with an ultramicrotome (Leica EM UC6 and put on a carbon-coated Nickel grid. Regular 2D projection images were obtained using a Tecnai 12 (FEI Co.) operating at 120 keV.

Scanning Transmission Electron Microscopy (*STEM*) *and Electron Energy Loss Spectroscopy* (*EELS*). STEM-EELS analysis was carried out using a FEI Titan Cryo Twin S/TEM performing at 300 kV, equipped with cryo-Twin objective lens, Gatan's Tridiem Image Filter and Digiscan-II as an external signal for STEM scanning. The microscope was set in STEM mode, magnification of 450K×, convergence angle of 10 mrad, spot size 8, gun lens of 6, and camera length 192 mm. Tridiem Image Filter was set in "spectroscopy" mode, dispersion of 0.05 eV, 0.1 s acquisition time. A spectrum offset of 20 eV was applied with collection angle of ∼16 mrad to acquire the STEM-EELS spectrum image from the area including an individual micelle. The STEM image was obtained using high-angle annular dark field (HAADF). STEM-EELS spectrum image was analyzed in Gatan's Software GMS 1.8.1. A power law background window of 20 eV was placed just before the Cu M2,3 edge at 75 eV, whereas a signal window of 8 eV (75−83 eV) was placed to sum the Cu M2,3 signal. The integrated signal is shown in the Figure 4e and shows the presence of Cu very clearly around the spherical micelles in the membrane.

Results and Discussion

Morphology of Pristine Block Copolymer Porous Films. Porous films prepared with commercial PS-*b*-P4VP diblock copolymer by following previously reported procedures[13] do not have an ordered structure relevant for membrane application. This has been confirmed by field emission scanning electron micrograph (FESEM) as depicted in Figure 1a. The pores are random, the porosity is low, and the cross-section morphology (Figure 1b) does not reflect a preferential order. Only the full comprehension of the sophisticated process of morphology formation in block copolymer systems offered the key to the development of this next generation membranes.

Block copolymers dissolved in selective solvents form micelles or other supramolecular structures[17−22] even without

Table 1. Values of Solubility Parameter, Dielectric Constant, and Donor Numbers for Different Solvents and Polymer Segments

			δ [MPa]$^{1/2}$ [b]			
	DN[a]	ε[a]	δ_D	δ_P	δ_H	$\delta = (\delta_D^2 + \delta_P^2 + \delta_H^2)^{1/2}$
styrene			18.6	1.0	4.1	19.1
pyridine	33.1	12.3	19.0	8.8	5.9	21.8
THF	20.0	7.6	16.8	5.7	8.0	19.5
DMF	26.6	36.1	17.4	13.7	11.3	24.9
water	18.0	81.0	15.5	16.0	42.3	47.8

[a] Reference 32. [b] Reference 33.

metal ions, depending on concentrations, block−block and block−solvent interactions, and the ratio of block lengths. Elongated structures on the film surface can be seen in Figure 1. No particular order is seen on the cross section of the film (Figure 1b). A first estimation of the polymer−solvent interactions can be performed with solubility parameters (Table 1).

THF is a good solvent (similar solubility parameter, δ) for the styrene block, while DMF is the preferred solvent for the pyridine block, which has δ higher than styrene. Most aggregates formed by self-assembly of amphiphilic block copolymers in selective solvents consist of a spherical core and a coronal shell. When a PS-*b*-P4PV block copolymer is dissolved in a 1:2 THF:DMF mixture, the styrene blocks assemble, tending to avoid unfavorable contacts with the DMF-rich medium. The pyridine blocks are preferentially exposed to the solvent. When the solution is cast and THF evaporates, the quality of the solvent medium changes continuously, becoming even more favorable for the P4VP block. The formation of micelles with styrene block cores and pyridine corona is stimulated. As the size of the insoluble block increases, the preferred structure can change to cylinders and vesicles in order to minimize the free energy. An excellent review on block copolymer morphology in solution has been recently published by Hayward and Pochan.[16]

During the membrane formation as THF is evaporated the top layer becomes much more concentrated and the micelles tend to pack, assuming a more ordered assembly. At the same time viscosity increases, contributing to the stability of the assemblies.

Copper−Block Copolymer Complex. When developing nanoporous films, monodispersed pore size distribution is an important goal. Aiming at membrane application, pores must also be accessible for fast transport across the film. High density of cylindrical channels perpendicular to the membrane surface is practically the best morphology for that. However, this is frequently not the morphology expected in the thermodynamic equilibrium. The key issue to use self-assembly of block copolymers to develop porous films is therefore the ability to direct and stabilize the aimed morphology, even far from equilibrium. This is the first time that metal complexation, block copolymer and phase inversion are used together for membrane preparation. With help of advanced microscopy methods we demonstrate here that metal−block copolymer complexes are an exceptional strategy for forming highly ordered porous films. Copper salts preferentially interact to one of the polymer blocks and act as a structure-directing and stabilizing agent, leading to a radical change of morphology (Figures 2 and 3). Very regular pores can be obtained (Figure 2). By analyzing the cross-section, contrary to the film produced without copper salt (Figure 1), an exceptionally well-ordered structure with channels perpendicular to the surface appears in the top layer (ca. 400 nm thick) (Figure 3). Although copper act as an ionic cross-linker between micelles, when water enters the solution during the phase inversion process, the intermicellar space is still the path of smallest resistance,

Scheme 1. Structure of Copper Complexes with 4-Pyridine Groups of Block Copolymer Chains and Acetate Anions Originally Forming the Copper Salt[23]

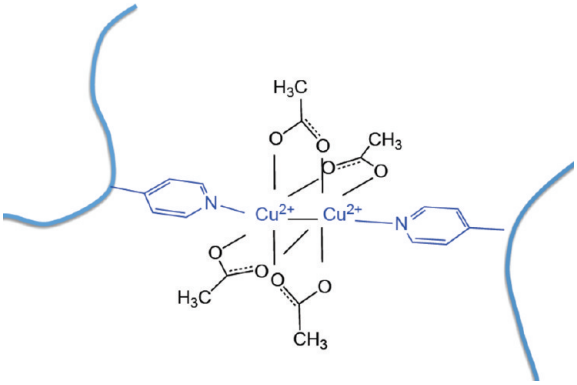

consolidating cylindrical channels, which are solidified as soon as the solvent-exchange proceeds.

Copper ions are known to form complex with pyridine groups.[23,24] The lone electron pair on nitrogen acts as a strong ligand for coordination with transition metals. Using copper acetate part of the acetate anions might remain complexed with copper, as confirmed for the analogous P4VP homopolymer by Belfiore and McCurdie[17] (Scheme 1), using spectroscopic methods. They also reported the shift of glass transition temperature of P4VP to higher values by the compexation with increasing amounts of metal ions, an evidence of strong interaction and physical cross-linking.

Solvents can also considerably affect the metal−polymer complex formation, by allowing or hindering the dissolution of metal salts and ligands and eventually also competing with the ligand in the complex formation. The solvent dielectric constant, ε, gives information on its ability of solvation by means of electrostatic interaction. Some values are listed in Table 1. DMF has a high value and is more likely to solve the salts. Solvation is also highly influenced by the solvent basicity or donor ability, which can be roughly estimated by the donor number (DN), defined as the negative enthalpy of reaction of a base with the Lewis acid antimony pentachloride.

As shown in Table 1, DMF has a DN value much nearer to that of pyridine than THF. This goes along with the values of solubility parameters for pyridine blocks and DMF, which are very similar. The ability of DMF to interfere or compete with pyridine in complex formation is expected to be higher than that of THF.

Focused Ion Beam Microscopy (FIB). FIB has been much less applied to polymers than to ceramic or metallic materials. Only recently the method has been used for membrane characterization.[25] However, this is a very versatile method, which can reveal much more information than considered up to now. In this paper we use FIB for the first time to obtain a 3D reconstruction of the membrane pore structure, by cutting a series of 150 membrane slices (Figure 3b) and setting the information together with image visualization software. The result can be seen in Figure 3c. The ordered top layer observed by FESEM in Figure 3a indicated the presence of aligned cylinders perpendicular to the surface. FIB also shows an aligned structure in the upper layer but gives evidence that the imperfect cylinders are indeed interconnected spherical cavities, which might be formed as a result of micelle regular packing (Figure 3b).

Cryo-Microscopy of Micelles in Solution. Micelle formation prior to immersion in water was confirmed by cryo-transmission electron microscopy (cryo-TEM) (Figure 4a)

and by cryo-FESEM (Figure 4b). The Cu^{2+} ions are preferentially located in the micelle corona (darker contour) as well as partially dispersed in the DMF-rich solvent with high dielectric constant. Micelles of diameter between 20 and 70 nm are visible (Figure 4b) and kept stable by the complexation. The micelle formation follows the thermodynamic expectations with the P4VP corona exposed to the polar solvent mixture rich in DMF and protecting the PS blocks from unfavorable interaction.

Stabilization of Micellar Structure. As mentioned before, micelle formation is commonly observed in block copolymer systems in solution.[26] However, for the method applied in this paper it is very important to stabilize the micellar structure and make use of this morphology for the formation of films with regular pores. When Cu^{2+} is added to the same system as depicted in Figure 1, spherical assemblies predominate until the final stages of membrane formation, as shown by transmission electron microscopy in Figure 4c,d. Metal-stabilized micelles organize in regularly packed spherical structures above a critical concentration, as the solvent evaporates, as depicted in Figure 3a. Christian et al.[27] have recently described the use of metal ions complexes with copolymers containing carboxylic groups to stabilize micelle assemblies. When the solution film is immersed in water an extremely fast water−solvent exchange occurs, the thermodynamic interaction between solvent and block copolymer decreases and the top layer gels, freezing the morphology. If the entropic and enthalpic factors controlling the segregation in solution are not strong enough, the system could be considerably disturbed during the immersion in water. Macrophase separation occurs, forming a disordered porous substrate (lower part of Figure 3a). Cu^{2+} adds stability to the self-assembled structure, acting as physical cross-linker between micelle coronas. This physical cross-link between micelles adds also mechanical strength to the final porous film. The presence of copper in the micelle improves the contrast in the transmission microscopy of the polymer film after immersion in water. The darker spots are richer in Cu^{2+} and thus have a higher electron density (Figure 4c). The spheres are arranged as a "pearl necklace", resembling structures reported for PS-*b*-polyacrylic solutions in the presence of Ca^{2+}.[17] Figure 4d was obtained by conventional HAADF-STEM. By choosing a specific micelle, low-loss EELS[28] was performed along a line shown in Figure 4d. The background removed M23 ionization edge signal of copper 74 eV along the line containing a micelle is integrated and shown in Figure 4e, confirming the preferential positioning of copper inside the micelle.

WAXS and SAXS Characterization. The morphological investigation of porous films prepared with copper−block copolymer complexes was completed with wide-angle (WAXS) (Figure 5a) and small-angle synchrotron X-ray scattering analysis (SAXS) (Figure 5b). Polystyrene and polyvinylpyridine have similar WAXS patterns. Two amorphous peaks have been previously reported for the homopolymers complexes with zinc salts.[29] The first peak at lower diffraction angle is due to the intermolecular distance between the polymer chains; the second peak at higher diffraction angle is related to the interphenyl (or pyridine) group distance. For P4VP homopolymer the interchain distance has been reported as 0.86 nm with a distance of 0.40 nm between pendant pyridine groups. By adding zinc salt, the distance between pendant groups is reduced. The coordination with zinc salt works like a physical cross-link and decrease also the interchain distance.

In our case the measured interchain distance was 0.870 ± 0.004 nm for the PS(138K)-*b*-P4VP(41K) copolymer.

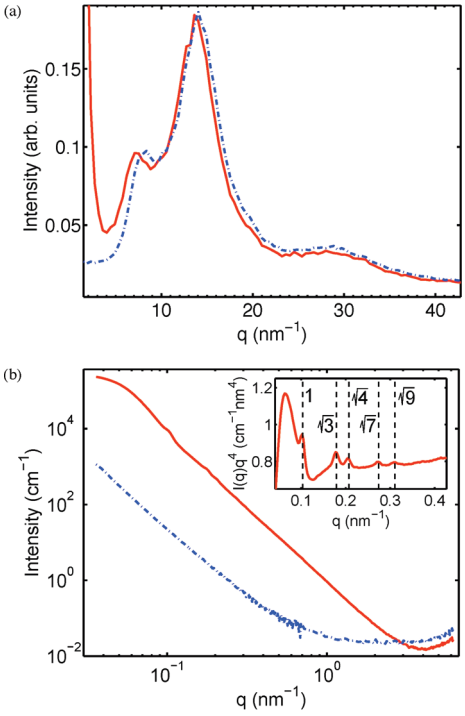

Figure 5. (a) WAXS and (b) SAXS analysis of membranes prepared of (—) PS-*b*-P4VP copolymers and (---) P4VP homopolymer. The inset shows the theoretical positions of reflections from a 2D hexagonal lattice with lattice parameter a = 70 nm.

A similar analysis for the P4VP homopolymer complexed with copper salt led to a value of 0.790 ± 0.002 nm. The distance between pendant groups was 0.457 ± 0.001 nm for the complexed copolymer and 0.446 ± 0.001 nm for the homopolymer. The lower interchain distance for the P4VP homopolymer can be easily understood, since the amount of complexing pendant groups is much larger. The copolymer contains only 23 wt % of complexing (P4VP) units, and it therefore has a lower density of cross-links with the copper salt. A third much broader scattering peak appears at 0.215 ± 0.001 and 0.220 ± 0.001 nm for copolymer and homopolymer films, respectively.

X-ray absorption near-edge spectroscopy (XANES) measurements showed that the samples contained copper but no distinct intensity changes were seen in the SAXS curves as a function of energy near the copper K-edge. This might be because the scattering pattern is resulting mainly from the regular arrangement of pores and not from the self-assembly of copper-containing micelles, which give to a weaker scattering contrast. The SAXS scattering curve (Figure 5b) for the PS-*b*-P4VP block copolymer porous film could be perfectly fitted with a 2D hexagonal lattice model.

This confirms the presence of cylindrical channels perpendicular to the film surface, with hexagonal order. The projection of these cylinders on a plane follow the drawing depicted in Figure 2.

The distance between cylinder centers evaluated using SAXS data was 70 nm, practically the same value estimated by scanning electron microscopy (Figure 2 and other higher magnification micrographs). The pores are highly ordered only in the upper 400 nm membrane layer (see Figure 3a). Although nonordered pores are present in the rest of the membrane, their average pore size is much larger, scattering at much lower q values. The P4VP homopolymer samples were prepared by complete solvent evaporation and are nonporous. Scattering in the SAXS region has much lower intensity.

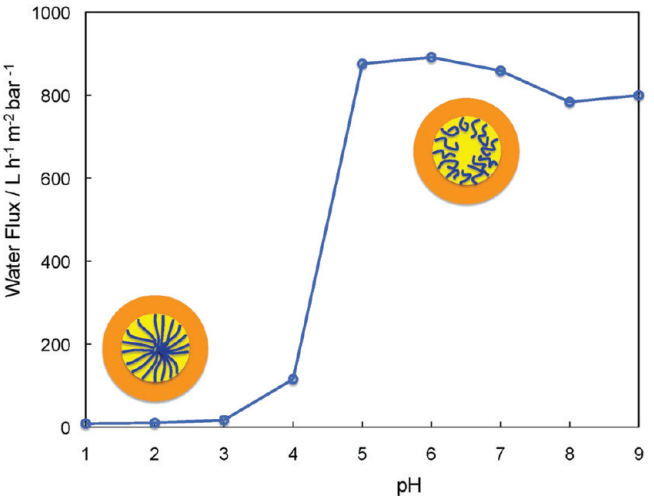

Figure 6. Water flux response to pH, measured at 1 bar feed pressure.

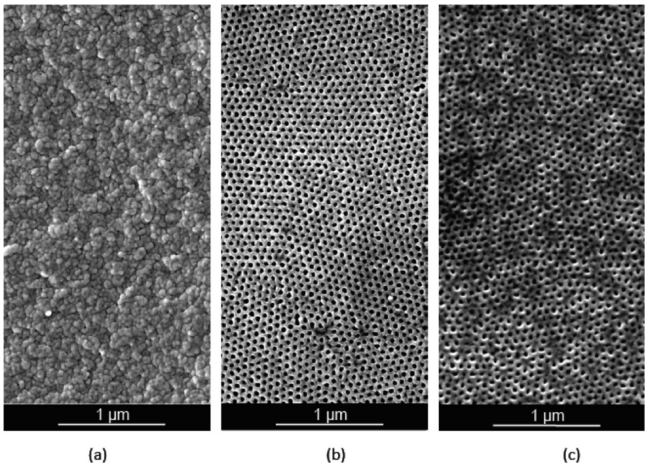

Figure 7. Porous films cast from 20 wt % PS-*b*-P4VP solutions with THF/DMF mixed solvent and 0.15 wt % $Cu(Ac)_2$ immersed in water after ca. 20 s THF evaporation. THF concentration: (a) 3, (b) 24, and (c) 32 wt %.

The FIB image shown in Figure 3b indicates that the cylindrical channels in the ordered top layer might be formed by spherical interconnected cavities. Spheres with a Gaussian size distribution with a hard-sphere structure factor were fitted separately, giving a mean sphere diameter of 62 nm with a standard deviation of 24 nm. However the 2D hexagonal arrangement of cylinders gave a better fitting than the best spherical arrangement (body-centered cubic) tested

Water Flux and pH Response. The surface pore density shown in Figure 2a,b is extremely high, around 2.3×10^{10} pores cm^{-2}. Figure 2b shows the very regular surface of the film cast on polyester nonwoven, according to the usual procedure for technical manufacture of polymeric asymmetric porous membranes.[31] This confirms that the membrane production can be easily scaled up. 10 cm × 50 cm large membranes were manufactured by using no much more than 2 g of copolymer dissolved and cast on polyester nonwoven. Roles of the same nonwoven and blades with comparable gate heights can be used in a small membrane machine for continuous film manufacture. There is only one technically available polymeric membrane with narrow distribution of pore sizes, which is obtained by track etching. A 30 nm track-etched polycarbonate membrane based on a previously reported electron micrograph[30] is depicted in Figure 2c.

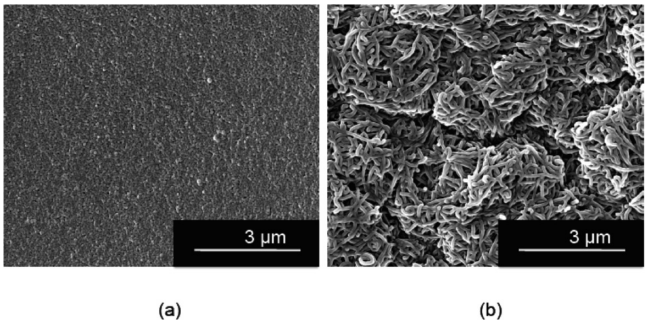

Figure 8. Porous films cast from 15 wt % PS-*b*-P4VP solutions in DMF/THF with 0.15 wt % $Cu(Ac)_2$ immersed in water after (a) 5 and (b) 75 s evaporation.

Porosity is clearly lower than with the new preparation process. Low porosity and random pore distribution has made the use of track etching membranes as template to grow nanowires ineffective, when aiming at electronic applications.[4,5]

Now considering membrane application for water purification, due to the ultrahigh pore density the water flux through these membranes has an extremely large value of about 890 L m^{-2} h^{-1} bar^{-1}, measured with deionized water at pH 7 and 1 bar. At pH 3 the water flux decreases to 10 L m^{-2} h^{-1} bar^{-1}, confirming another exciting property of this membrane—its stimuli response (Figure 6). The pores can reversibly close or open as a pH-sensitive gate. The pyridine groups are protonated at low pH and the blocks extend to minimize charge repulsion, transforming the pores into a pH-sensitive gate.

Furthermore, the coexistence of hydrophobic (styrene-rich) nanoregions, pores coated by hydrophilic (P4VP-rich) segments, and copper ions could offer an effective strategy against fouling, which is one of the largest issues affecting the performance of membranes for water treatment.

After the process optimization on glass plates, the film preparation was scaled up for manufacture on polyester nonwoven increasing its mechanical stability for further application and facilitating the production in larger scale in a technical machine.

Influence of Solvent Composition and Evaporation Time. Films were prepared with casting solutions originally with different THF concentrations. THF is the most volatile solvent in the THF/DMF mixture. If the THF concentration is low (Figure 7a), the concentration near the surface does not increase enough before immersion in water. The system seems to reach a maximum order using solutions with 24 wt % THF (Figure 7b). When the THF concentration (Figure 7c) is higher, also high order is observed, but less than in the previous case. This might be due to excessive increase of viscosity with THF complete evaporation. The mobility becomes too low to allow optimal packing.

By changing the evaporation time from 3 to 20 and 40 s, using 20 wt % copolymer casting solution with 56 wt % DMF, 24 wt % THF, and 0.15 wt % $Cu(Ac)_2$, a slight increase of order was observed. When using less viscous 15 wt % copolymer solutions, a dramatic change of morphology was observed (Figure 8). By increasing the time of THF evaporation, wormlike morphology was favored instead of regular pores.

Conclusion. We developed a new method for the preparation of ultrawater-permeable and pH-responsive asymmetric porous membranes, using a combination of block copolymers and metal complexation. This new technique is integrated in a classical process of phase separation, easily up-scalable for industrial membrane casting equipment. A detailed

morphological investigation using cryo-TEM, FESEM, cryo-FESEM, HAADF-STEM, EELS, FIB, WAXS, and SAXS made possible to fully understand the mechanism of porous film formation. The role of supramolecular micelle assembly in the pore formation had been completely ignored before.[13] With this knowledge and by adding metal ions to stabilize the micelles assembly, a large step forward could be done leading to much more reproducible membranes with better controlled morphology. Also long-range order was confirmed. Nevertheless, to our knowledge, this study presents the first reported production of reproducible stimuli-sensitive membranes with high porosity and monodispersed pores for nanofiltration and ultrafiltration, a range relevant for water contaminants caused by human activity like hormones, antibiotics, and endocrine disrupters. This technological advance opens an exceptional variety of opportunities for water purification, medical and pharmaceutical applications, and templates for electronic industry.

Acknowledgment. We thank Kun Li from the KAUST Core Lab for Advanced Nanofabrication, Imaging and Characterisation for his support for the morphological characterization. We thank Prof. G. Wegner from the Max-Planck-Institute Mainz for helpful discussions.

References and Notes

(1) Nunes, S. P., Peinemann, K.-V., Eds. *Membrane Technology*; Wiley-VCH: Weinheim, Germany, 2010; Vol. *4*.
(2) Shannon, M. A.; Bohn, P. W.; Elimelech, M.; Georgiadis, J. G.; Marinas, B. J.; Mayes, A. M. *Nature* **2008**, *452*, 301–310.
(3) Nunes, S. P., Peinemann, K.-V., Eds. *Membrane Technology*; Wiley-VCH: Weinheim, Germany, 2007; Vol. *1*.
(4) Park, S.; Wang, J.-Y.; Kim, B.; Xu, J.; Russell, T. P. *ACS Nano* **2008**, *2*, 766–772.
(5) Thurn-Albrecht, T.; Schotter, J.; Kästle, G. A.; Emley, N.; Shibauchi, T.; Krusin-Elbaum, L.; Guarini, K.; Black, C. T.; Tuominen, M. T.; Russell, T. P. *Science* **2000**, *290*, 2126–2129.
(6) Hamley, I. W. *Nanotechnology* **2003**, *14*, R39–R54.
(7) Bates, F. S.; Fredrickson, G. H. *Phys. Today* **1999**, *52*, 32–38.
(8) Lehn, J. M. *Supramolecular Chemistry*; Wiley-VCH: Weinheim, Germany, 1995.
(9) Phillip, W. A.; Martono, E.; Chen, L.; Hillmyer, M. A.; Cussler, E. L. *J. Membr. Sci.* **2009**, *337*, 39–46.
(10) Ikkala, O.; ten Brinke, G. *Science* **2002**, *295*, 2407–2409.
(11) Sidorenko, A.; Tokarev, I.; Minko, S.; Stamm, M. *J. Am. Chem. Soc.* **2003**, *125*, 12211–12216.
(12) Yang, S. Y.; Ryu, I. C.; Kim, H. Y.; Kim, J. K.; Jang, S. K.; Russell, T. *Adv. Mater.* **2006**, *18*, 709–712.
(13) Peinemann, K.-V.; Abetz, V.; Simon, P. F. W. *Nature Mater.* **2007**, *6*, 992–996.
(14) Bang, J.; Jeong, U.; Ryu, D. Y.; Russell, T. P.; Hawker, C. J. *Adv. Mater.* **2009**, *21*, 4769–4792.
(15) Jackson, E.; Hillmyer, M. A. *ACS Nano* **2010**, *4*, 3548–3553.
(16) Hayward, R. C.; Pochan, D. J. *Macromolecules* **2010**, *43*, 3577–3584.
(17) Discher, D. E.; Eisenberg, A. *Science* **2002**, *297*, 967–973.
(18) Smart, T.; Lomas, H.; Massignani, M.; Flores-Merino, M. V.; Ruiz Perez, L.; Battaglia, G. *Nano Today* **2008**, *3*, 38–46.
(19) Rodriguez-Hernande, J.; Checot, F.; Gnanou, Y.; Lecommandoux, S. *Prog. Polym. Sci.* **2005**, *30*, 691–724.
(20) Battaglia, G.; Ryan, A. J. *Nature Mater.* **2005**, *4*, 869–876.
(21) Min, Y.; Akbulut, M.; Kristiansen, K.; Golan, Y.; Israelachvili, J. *Nature Mater.* **2008**, *7*, 527–538.
(22) Zhang, L.; Yu, K.; Eisenberg, A. *Science* **1996**, *272*, 1777–1779.
(23) Belfiore, L.; McCurdie, M. P. *J. Polym. Sci., Part B: Polym. Phys.* **1995**, *33*, 105–124.
(24) Santana, A. L.; Giacomelli, C.; Oliveira, P. N.; Pires, A. T. N.; Bertolino, J. R.; Spinelli, A. *J. Polym. Sci., Part B: Polym. Phys.* **2009**, *47*, 215–225.
(25) Boussu, K.; De Baerdemaeker, J.; Dauwe, C.; Weber, M.; Lynn, K. G.; Depla, D.; Aldea, S.; Vankelecom, I. F. J.; Vandecasteele, C.; Van der Bruggen, B. *ChemPhysChem* **2007**, *8*, 370–379.
(26) Siqueira, D. F.; Nunes, S. P.; Stamm, M.; Wolf, B. A. *Macromolecules* **1994**, *27*, 4561–4565.
(27) Christian, D. A.; Tian, A.; Ellenbroek, W. G.; Levental, I.; Rajagopal, K.; Janmey, P. A.; Liu, A. J.; Baumgart, T.; Discher, D. E. *Nature Mater.* **2009**, *8*, 843–849.
(28) Egerton, R. F. *Electron Energy-Loss Spectroscopy in the Electron Microscope*; Plenum Press: New York, 1996.
(29) Kuo, S. W.; Wu, C.-H.; Chang, F.-C. *Macromolecules* **2004**, *47*, 192–200.
(30) Savariar, E. N.; Krishnamoorthy, K.; Thayaumanavan, S. *Nature Nanotechnol.* **2008**, *3*, 112–117.
(31) Baker, R. W. *Membrane Technology and Applications*; John Wiley & Sons: Chichester, 2004.
(32) Huheey, J. E. *Inorganic Chemistry*; Harper and Row: London, 1975.
(33) Hansen, C. M. *Solubility Parameters: a User's Handbook*; CRC Press: Boca Raton, FL, 2000.